frontiers in Earth Science

ORIGINAL RESEARCH
published: 26 March 2019
doi: 10.3389/feart.2019.00058

Structure of Lō'ihi Seamount, Hawai'i and Lava Flow Morphology From High-Resolution Mapping

David A. Clague[1], Jennifer B. Paduan[1], David W. Caress[1], Craig L. Moyer[2], Brian T. Glazer[3] and Dana R. Yoerger[4]*

[1] Monterey Bay Aquarium Research Institute, Moss Landing, CA, United States, [2] Department of Biology, Western Washington University, Bellingham, WA, United States, [3] Department of Oceanography, University of Hawai'i, Honolulu, HI, United States, [4] Applied Ocean Physics and Engineering, Woods Hole Oceanographic Institution, Woods Hole, MA, United States

The early development and growth of oceanic volcanoes that eventually grow to become ocean islands are poorly known. In Hawai'i, the submarine Lō'ihi Seamount provides the opportunity to determine the structure and growth of such a nascent oceanic island. High-resolution bathymetric data were collected using AUV *Sentry* at the summit and at two hydrothermal vent fields on the deep south rift of Lō'ihi Seamount. The summit records a nested series of caldera and pit crater collapse events, uplift of one resurgent block, and eruptions that formed at least five low lava shields that shaped the summit. The earliest and largest caldera, formed ∼5900 years ago, bounds almost the entire summit plateau. The resurgent block was uplifted slightly more than 100 m and has a tilted surface with a dip of about 6.5° toward the SE. The resurgent block was then modified by collapse of a pit crater centered in the block that formed West Pit. The shallowest point on Lō'ihi's summit is 986 m deep and is located on the northwest edge of the resurgent block. Several collapse events culminated in formation of East Pit, and the final collapse formed Pele's Pit in 1996. The nine mapped collapse and resurgent structures indicate the presence of a shallow crustal magma chamber, ranging from depths of ∼1 km to perhaps 2.5 km below the summit, and demonstrate that shallow sub-caldera magma reservoirs exist during the late pre-shield stage. On the deep south rift zone are young medium- to high-flux lava flows that likely erupted in 1996 and drained the shallow crustal magma chamber to trigger the collapse that formed Pele's Pit. These low hummocky and channelized flows had molten cores and now host the FeMO hydrothermal field. The Shinkai Deep hydrothermal site is located among steep-sided hummocky flows that formed during low-flux eruptions. The Shinkai Ridge is most likely a coherent landslide block that originated on the east flank of Lō'ihi.

Keywords: caldera, pit crater, landslide, channelized flows, hummocky flows, Lō'ihi Seamount

OPEN ACCESS

Edited by:
Carles Soriano, Instituto de Ciencias de la Tierra Jaume Almera (ICTJA), Spain

Reviewed by:
Sharon Allen, University of Tasmania, Australia
Alessandro Tibaldi, University of Milano-Bicocca, Italy

****Correspondence:***
David A. Clague
clague@mbari.org

Specialty section:
This article was submitted to Volcanology, a section of the journal Frontiers in Earth Science

Received: *27 August 2018*
Accepted: *08 March 2019*
Published: *26 March 2019*

Citation:
Clague DA, Paduan JB, Caress DW, Moyer CL, Glazer BT and Yoerger DR (2019) Structure of Lō'ihi Seamount, Hawai'i and Lava Flow Morphology From High-Resolution Mapping. Front. Earth Sci. 7:58. doi: 10.3389/feart.2019.00058

INTRODUCTION

The timing of development of shallow sub-caldera magma chambers and their overlying calderas remains uncertain in basaltic volcanoes. In Hawai'i, this uncertainty reflects disagreement about whether the summit plateau of the submarine Lō'ihi Seamount is a caldera complex. Lō'ihi Seamount is the youngest volcano in the nearly 8000 km-long Hawaiian-Emperor volcanic

chain that stretches across the north Pacific (Clague and Dalrymple, 1987). The seamount is located at the southeastern end of the Hawaiian Islands (**Figure 1**). Emery (1955) named Lōʻihi and presented the first of several bathymetric charts showing the north-south elongate shape of the volcano and suggested that Lōʻihi and nearby Papaʻu (**Figure 2**) might mark the locations of young submarine volcanoes related to the Hawaiʻian volcanic chain. It was not, however, until the Hawaiʻian Volcano Observatory's seismic network detected earthquake swarms in 1971–1972 and 1975 located beneath the volcano (Klein, 1982; Bryan and Cooper, 1995) that Lōʻihi was recognized as an active submarine volcano and the youngest in the Hawaiʻian-Emperor chain. That Lōʻihi was an active volcano was quickly confirmed when fresh, glassy lava samples were recovered (Moore et al., 1979, 1982; Frey and Clague, 1983; Garcia et al., 1989), and active hydrothermal vents and deposits were identified and sampled near the summit (Malahoff et al., 1982; De Carlo et al., 1983; Karl et al., 1988, 1989). Since that time, Lōʻihi has been the focus of intense study with numerous oceanographic expeditions and *Pisces IV and V, ALVIN, MIR*, and *Shinkai 6000* submersible and *Kaiko* and *Jason* remotely operated vehicle (ROV) dives that have collected samples and made visual and video observations. In 1996, an intense seismic swarm (Caplan-Auerbach and Duennebier, 2001a,b) accompanied the formation of a new pit crater named Pele's Pit (Lōʻihi Science Team, 1997) and initiation of sulfide/sulfate deposition inside it (Davis and Clague, 1998; Davis et al., 2003), and again invigorated scientific work at Lōʻihi. The formation of the summit pit crater in 1996 has renewed importance as summit collapse has recently occurred at Kīlauea Volcano.

The uncertainty about whether the summit of Lōʻihi Seamount is a caldera complex results from the prior lack of high-resolution bathymetry of the summit. This study presents and discusses results from three surveys done at different resolutions. The first is a GPS-navigated bathymetric survey collected in 2014 using a Simrad EM302 0.5° × 1° system on the R/V *Falkor*, operated by the Schmidt Ocean Institute (**Figure 2**). The second is a high-resolution deep-tow Reson 8101 sonar survey done in 1997 (**Figure 3**) to plan the cable route for the Hawaii Undersea Geological Observatory (HUGO) (Duennebier et al., 2002). The third, and highest resolution, is surveys by AUV *Sentry*, operated by Woods Hole Oceanographic Institution (e.g., **Figure 4**). The deep-tow and *Sentry* surveys required extensive post-processing to clean noise and adjust for navigation offsets; all the data could not be recovered, especially for the deep-tow survey. These high-resolution surveys, coregistered to the GPS-navigated EM302 survey collected by the R/V *Falkor* for the entire volcano, allow us to take a new and more detailed look at the morphology and structure of Lōʻihi Seamount, including the formation of Pele's Pit in 1996.

PREVIOUS WORK

Lōʻihi Seamount has been mapped repeatedly as mapping and navigation technologies improved. Despite the intensity of scientific research on Lōʻihi, detailed descriptions and discussion of its geomorphology and structure are largely based on visual or video observations and single sonar beam or low-resolution multibeam surveys. The earliest surveys were done by the U.S. Navy in the 1950s and formed the basis of the Emery (1955) identification and naming of Lōʻihi Seamount. The Navy also collected a multibeam survey using SASS (Malahoff et al., 1982; Malahoff, 1987). A single-beam survey in 1981 (Moore et al., 1982) located the seamount accurately and showed that the summit was generally flat at a depth slightly greater than 1000 m and had several collapse pits each several 100 m deep, as depicted in their **Figure 2** and in **Figures 6.3**, **6.4** in Malahoff (1987). Two sidescan surveys followed using the towed Sea MARK II (Smith et al., 1994) and the GLORIA system (Holcomb et al., 1988; Holcomb and Robinson, 2004). Much of this work, as well as most sampling of lava flows and hydrothermal deposits, was done before GPS navigation was available or available 24-h per day (Moore et al., 1982; Malahoff, 1987; Fornari et al., 1988; Chadwick et al., 1993). The initial surveys by Moore et al. (1982) and Malahoff (1987) were superior to some later surveys in that navigation was done using triangulation with a radar-frequency transponder positioning system from shore-based stations on the Island of Hawaii.

Modern GPS or differential GPS navigated multibeam surveys (MBARI Mapping Team, 2000; Smith et al., 2002; Eakins et al., 2004) were an important advance. The survey done in 1998 (MBARI Mapping Team, 2000) used a Simrad EM300 multibeam system and differential GPS for navigation, but the system provided coverage only as deep as 4000 m. At the summit, the resolution is ∼15–20 m. The seamount (**Figure 2**) was mapped again during a JAMSTEC program in 2000–2002 using Seabeam (Smith et al., 2002; Eakins et al., 2004), which provided GPS-navigated coverage of the entire seamount at similar resolution to the earlier EM300 survey.

The general structure of Lōʻihi Seamount was evident from the early surveys (Moore et al., 1982; Malahoff, 1987; Fornari et al., 1988; Karl et al., 1988; Chadwick et al., 1993). The volcano has a nearly flat summit platform at about 1000 m depth and two distinct rift zones that extend to the north and then northeast and to the south (**Figure 2**). The southern part of the summit platform was modified by two distinct collapse pits prior to the 1996 formation of Pele's Pit, a third summit pit crater (Lōʻihi Science Team, 1997). Constructional volcanic activity is concentrated along the rifts and at the summit, although rare volcanic cones occur away from the rift zones on the lower flanks, particularly the northwest flank (one was sampled by dredge 31 in Moore et al., 1982). The south rift extends ∼19 km to a depth of about 5000 m (average plunge of 10°) whereas the north rift is ∼11 km long and merges into the submarine slope of Mauna Loa volcano at a depth of about 2000 m (average plunge of 6°) (Fornari et al., 1988). The north rift zone consists of two roughly parallel ridges with the western one being the longer, more prominent one. Just north of the north rift zone, Papa'u (**Figure 2**) is not another young volcano as proposed by Emery (1955). It consists of uplifted and folded, poorly consolidated volcaniclastic sediments associated with the active Hilina fault zone on the south flank of Kīlauea Volcano (Moore and Chadwick, 1995; Morgan et al., 2003).

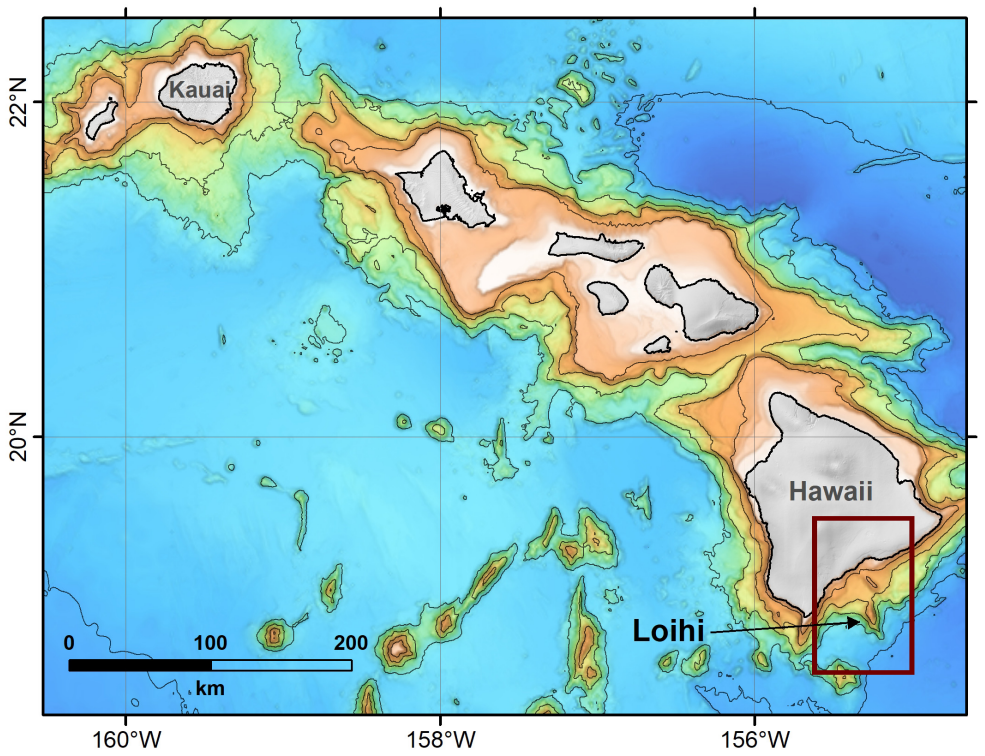

FIGURE 1 | Location map showing the Hawaiian Islands from Kaua'i to the northwest to Hawai'i at the southeast. Multibeam bathymetry around the islands is shown with one-km contours from 1 to 5 km below sea level. Lō'ihi Seamount is labeled and the box shows the extent of **Figure 2**.

The outer rim of the summit is generally shallower than the center. Malahoff (1987) interpreted this broad summit depression as a caldera, and Fornari et al. (1988) interpreted the elevated rim as a series of cones erupted through ring faults on the margin of the summit platform. The three summit pit craters have been explored during numerous submersible dives that have shown that all are steep-walled and expose sequences of truncated lava flows (Garcia et al., 1993; Lō'ihi Science Team, 1997). Pele's Pit collapsed beneath the former location of the low-temperature (up to 30°C) Pele's Vents hydrothermal field (e.g., Sedwick et al., 1992, 1994), and high-temperature (about 200°C) venting was found around the base of the pit walls after the collapse (Lō'ihi Science Team, 1997; Davis and Clague, 1998; Wheat et al., 2000; Davis et al., 2003). More recent observations (Glazer and Rouxel, 2009) indicate that these vents have cooled significantly and are no longer depositing sulfides and sulfates. Part of the summit platform, particularly the eastern half, is covered by volcaniclastic deposits up to 11 m thick (Clague et al., 2000, 2003; Clague, 2009; Schipper et al., 2011), which obscure the underlying lava flows and smooth the relief of the summit platform.

The rift zones and summit platform have asymmetric slopes to the east and west, which Malahoff (1987); Fornari et al. (1988), Moore et al. (1989), and Garcia et al. (2006) interpreted to be the headwalls of landslides that modified Lō'ihi's flanks. Two slumps have modified the west flank of Lō'ihi, whereas a much larger slide or merged slides (**Figure 2**) has modified the eastern flank (Malahoff, 1987).

Lava flows on Lō'ihi are described as mainly pillow lava, but knobby 'a'a-like blocky flows are also present, based on shape and surface textures of dredged fragments (Moore et al., 1982; and references cited in Garcia et al., 2006). The only papers focused on lava flow morphology (Umino et al., 2000, 2002) described inflation features of lobate and hollow or drained lobate flows observed on the deep south rift zone during *Kaiko* ROV dives 94 and 96 between ∼4050 and 4920 m depth. The deeper dive 96 (Umino et al., 2000, 2002) was located just uprift of a *Sentry* high-resolution survey of the FeMO hydrothermal site described below.

DATA AND DATA PROCESSING

We combine data from four surveys, each at different resolution. The broadest regional coverage of the deepest parts of the volcano (>4000 m depth) is based on several generations of SeaBeam data used in the Smith et al. (2002) compilation (**Figure 2**). Simrad EM302 bathymetric and backscatter data of the seamount collected from the R/V *Falkor* in 2014 are higher resolution than prior SeaBeam or the EM300 data (MBARI Mapping Team, 2000) and supplant those data. The EM302 survey mapped most of the edifice of Lō'ihi Seamount (**Figure 2**) at a resolution of ∼17 m at the summit and ∼85 m at 5000 m depth, but did not extend away from the base of the seamount nor cover the entire north rift or west flank, and in particular, the region of high-backscatter

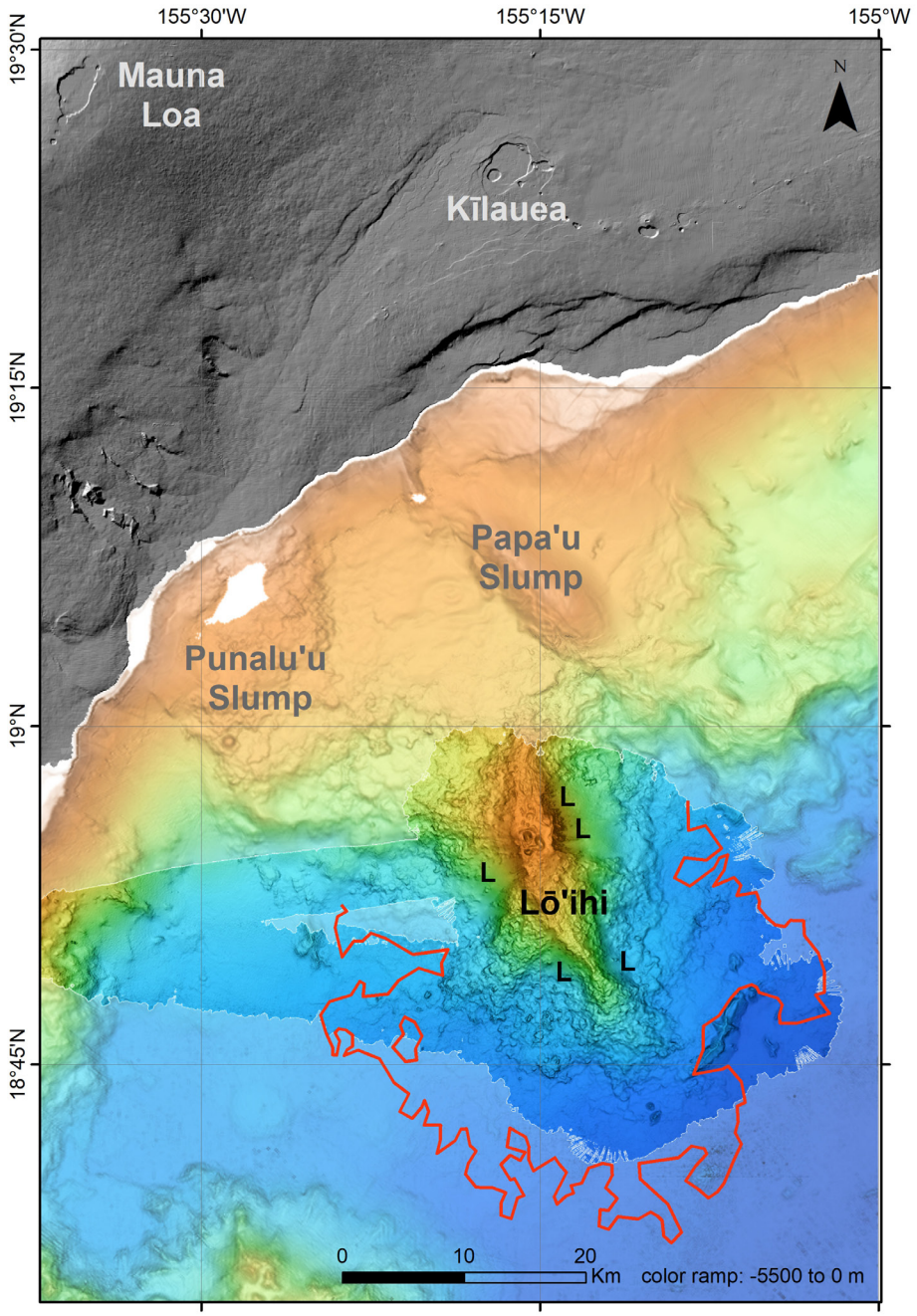

FIGURE 2 | Regional map of Lō'ihi Seamount, the surrounding seafloor, and the subaerial south flank of the island of Hawaii. Bright colored bathymetry indicates Simrad EM302 bathymetric data collected in 2014 from the R/V *Falkor* and gridded at 50 m. The underlying faded bathymetry is lower resolution data collected earlier (Smith et al., 2002). The summit calderas of Kīlauea and Mauna Loa are labeled, as are the Punalu'u and Papa'u slumps (Moore and Chadwick, 1995; Morgan et al., 2003). The red line surrounding Lō'ihi is the extent of high-backscatter lava flows (modified from Holcomb et al., 1988). The letter L indicates the locations of flank landslides on Lō'ihi Seamount. Color ramp for this and subsequent figures is blue for deep to orange for shallow.

inferred by Holcomb et al. (1988), based on GLORIA side-scan data (**Figure 2**), to consist of extensive flows from Lō'ihi Seamount was only partly mapped. We have coregistered the higher resolution surveys to the EM302 data (see below). The higher-resolution survey for the HUGO cable route (Duennebier et al., 2002) suffers from poor navigation and noisy data, but covers almost the entire summit and upper rift zones (**Figure 3**). These data were collected using a Reson 8101 (1.5° by 1.5° 240 kHz) multibeam mounted on a McCartney FOCUS steerable tow body operated by SAIC in 1997; only depth information could be recovered. The survey experienced abrupt depth and lateral offsets that could not be corrected and the navigation

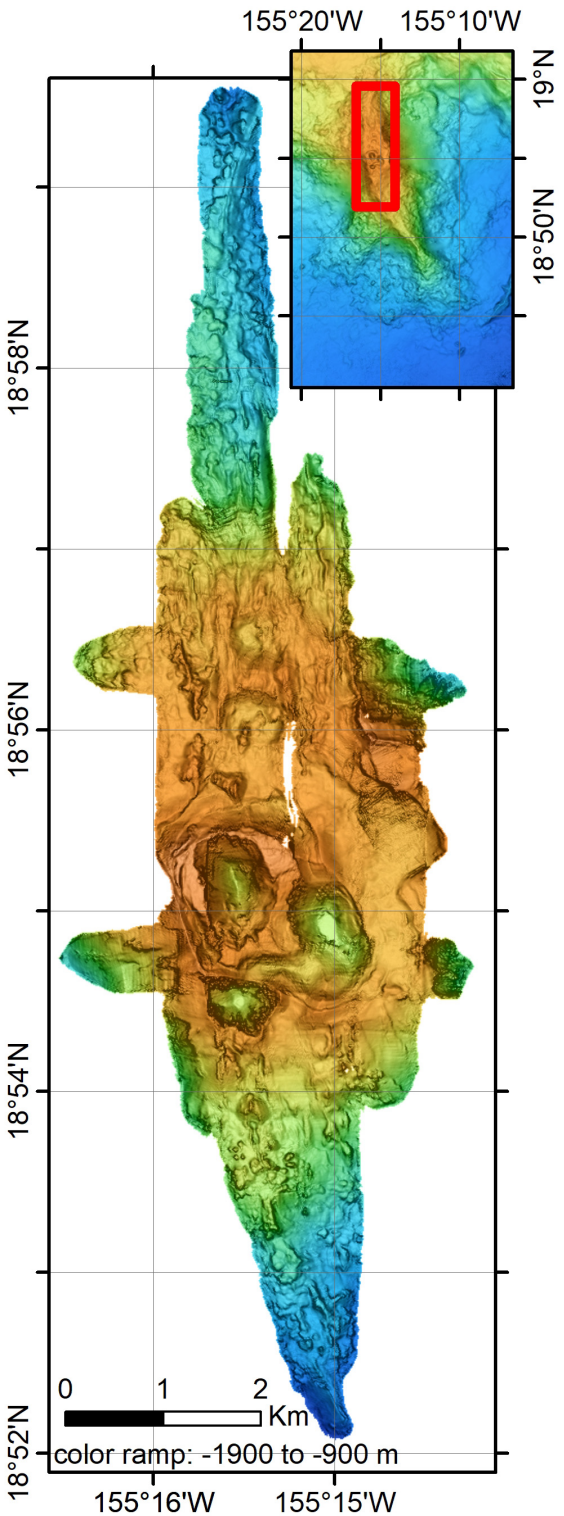

FIGURE 3 | Towed Reson bathymetric survey collected prior to laying the cable to the HUGO seafloor observatory. The survey was collected in 1998 by SAIC using a towed system with limited navigational control. The survey has been adjusted to be co-located with the EM302 GPS-navigated data collected in 2013. Not all data from this survey could be re-located.

(Continued)

FIGURE 3 | Continued

In addition, the swaths on the north rift could not be matched to the underlying ship data and are either mislocated by being too far west or have a depth offset of about 50 m to deeper depths. The map is gridded at 10 m.

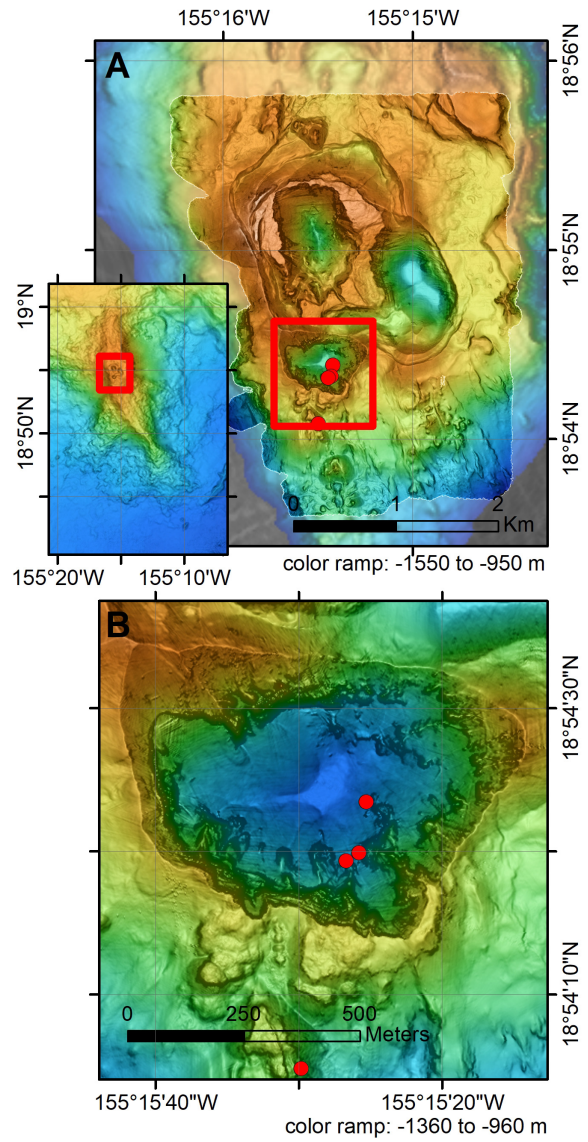

FIGURE 4 | (A) AUV *Sentry* multibeam bathymetry showing the combined map of missions 164–172, [except 168 and 170] of Lō'ihi's southern summit platform collected in 2013. The red box is the extent of **(B)**. **(B)** Close up of Pele's Pit showing the scalloped margin and ridges perpendicular to the rim. The three red dots are the locations of known vent fields inside Pele's Pit. The data are gridded at 5 m instead of the 1.5 m resolution of individual swaths. Pele's Pit data are gridded at 2 m and background Simrad EM302 data are gridded at 20 m.

coregistration to underlying EM302 data is less reliable than usually attained for AUV high-resolution map data, so it is best gridded at about 10 m cell size.

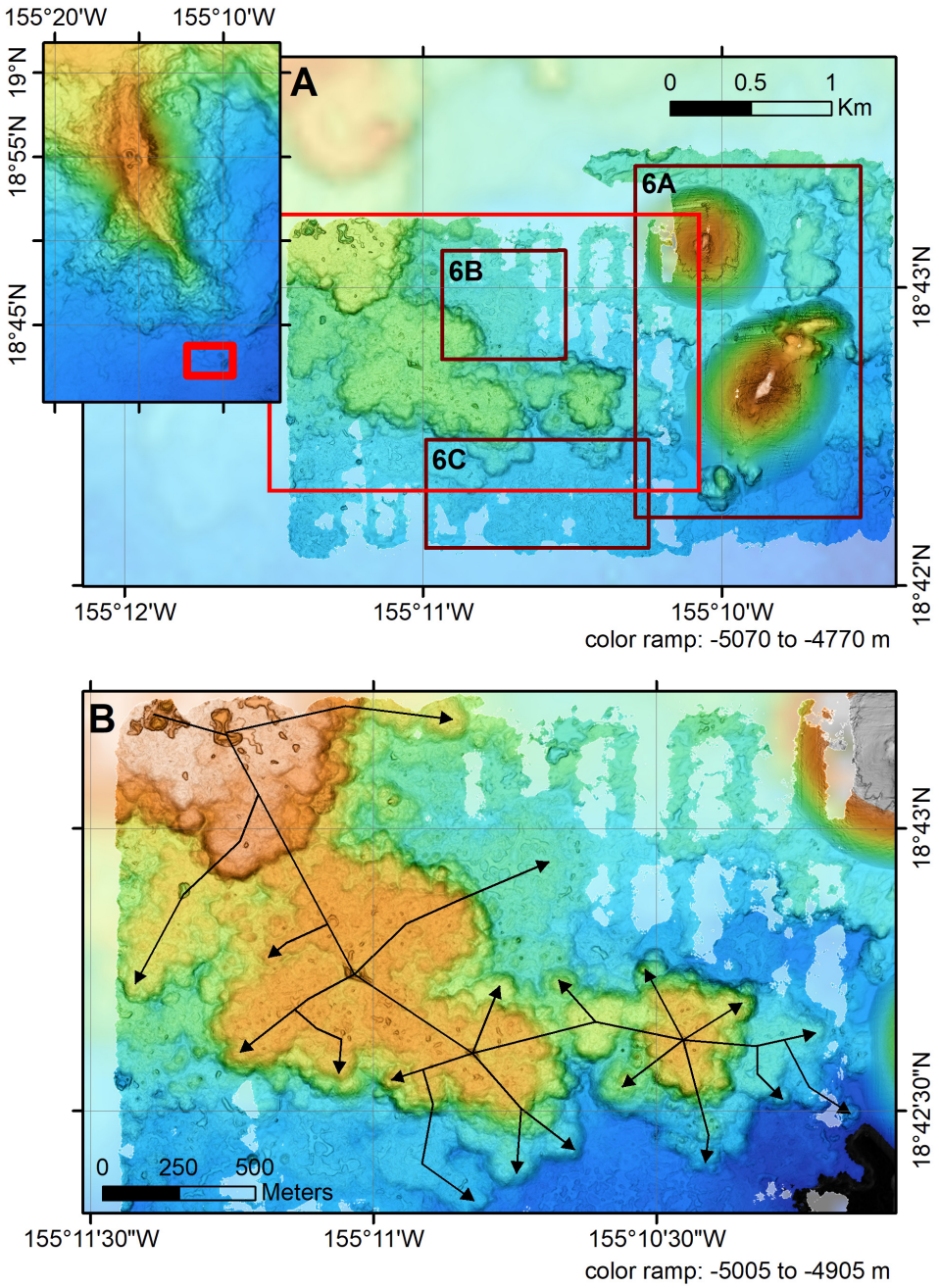

FIGURE 5 | (A) AUV *Sentry* multibeam bathymetry showing the combined map of missions 168, 264, and 265 of the FeMO hydrothermal site collected in 2013 and 2014. Boxes show extents of part **(B)** and **Figures 6A–C**. **(B)** Close-up of hummocky flows with arrows showing how lava advanced within the flow. The yellow-colored mound to the east has a shallower depth than the flows above the tube that fed it.

The highest resolution data for the southern portion of summit region were collected during 7 AUV surveys (164–172, except 168 and 170) using *Sentry* in 2013 (**Figure 4**). The Reson 7125 multibeam sonar on *Sentry* has a resolution of about 1.5 m when routinely flown at an altitude of ∼60 m. Additional AUV *Sentry* surveys were conducted on the distal south rift zone at the FeMO hydrothermal site (Edwards et al., 2011) in 2013 and 2014 during *Sentry* missions 168, 264, and 265 (**Figures 5**, **6**). Part of survey 265 over the FeMO venting area, collected at an altitude of only 5 m, has roughly 5 cm resolution (**Figure 6D**) and collected overlapping bottom photographs (**Figure 7**). AUV *Sentry* surveys were also completed at the Shinkai Deep hydrothermal site during missions 266 and 270 and at the Shinkai Ridge site during missions 267 and 269 (**Figures 8**, **9**). The increasingly higher-resolution surveys cover smaller and smaller areas nested within the Simrad EM302 surveys.

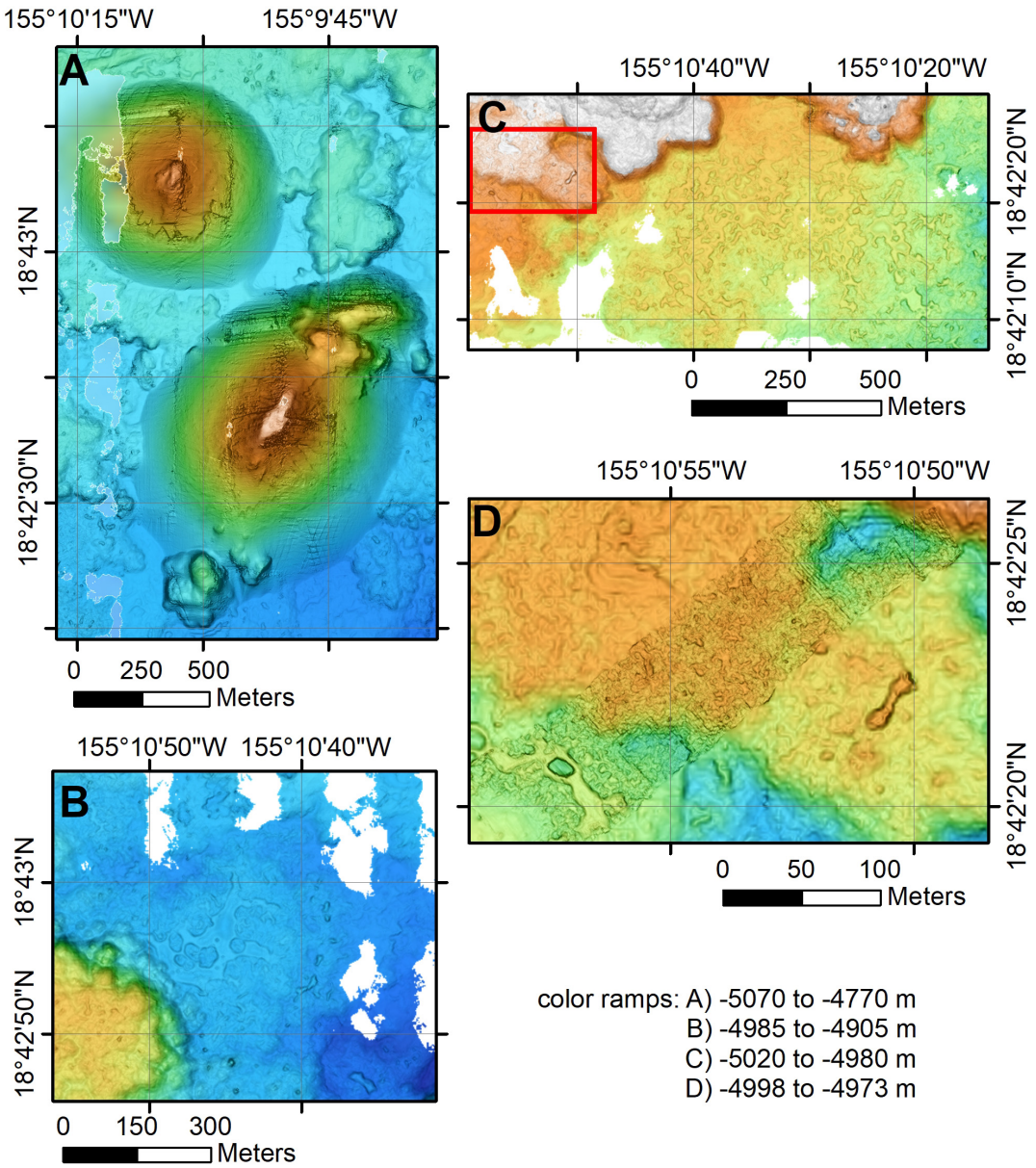

FIGURE 6 | (A) Detail of the two cones (southern one is ~300 m tall and 160 by 260 m across at the base) with smooth slopes located on the extension of the south rift. Resolution is 2 m. **(B)** Detail close-up of channelized flow with abundant drainback features. This flow originates at the edge of the hummocky flow lobe to the southwest. **(C)** Detail of another channelized flow with abundant drainback features that started from the hummocky flow lobe to the north. These rapidly emplaced flows are the molten cores of the hummocky flows that presumably reflect increased flux as the eruption proceeded. Extent of maps A, B, and C are shown by boxes on **Figure 5A**. **(D)** A portion of *Sentry* Reson bathymetric mission 265 of the FeMO hydrothermal site that was collected from an altitude of just 5 m. Bathymetry has about 5 cm resolution and overlapping photographic coverage (representative images in **Figure 7**). Individual lobate flow lobes a few m across can be seen, as can a small drained lava pond in a channelized flow in the southwest corner of the map. Extent of the map shown by box in part **(C)**. Each map is at a different scale and with a different depth range to highlight the details.

The *Sentry* and deep-tow data were reprocessed using MB-System (Caress and Chayes, 2011). Data editing used the 3-D mbeditviz tool and re-navigation used the mbnavadjust tool, first on individual surveys and then on combined surveys as multi-mission mbnavadjust projects for the summit and deep south rift, and then tying to points in the better-located EM302 survey.

RESULTS

General Bathymetric Characteristics

The overall structure of Lō'ihi Seamount (**Figure 2**) is largely as previously described (e.g., Malahoff, 1987; Fornari et al., 1988). The summit is a flat platform that connects to a ~15 km long northern rift and a 22-km long curved south rift. No radial

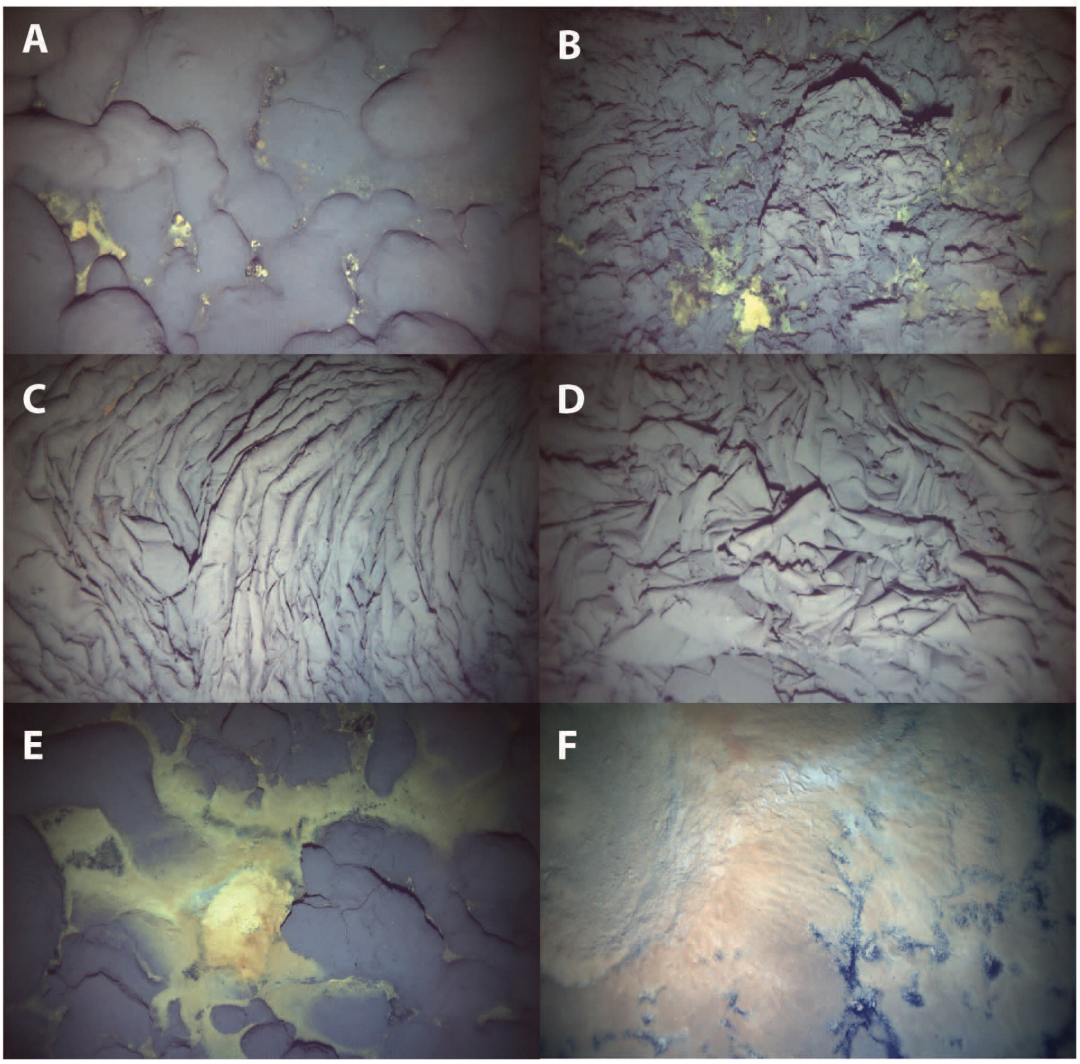

FIGURE 7 | Photographs collected by AUV *Sentry* during low-altitude portion of mission 168. No lasers were utilized to provide accurate scale, but the images are ~3–5 m across. **(A)** Pillow lava with minor hydrothermal sediment between pillows at 18.70781° latitude, –155.18420° longitude, and 4977 m depth. **(B)** Jumbled sheet flow with minor yellow hydrothermal sediment. 18.70795°, –155.18443°, 4975 m. **(C)** Drapery folded sheet flow at 18.70747°, –155.18493°, 4976 m. **(D)** Drapery folded to jumbled sheet flow. **(E)** Pillow lava with abundant yellow hydrothermal sediment and bacterial mat at 18.70769°, –155.18375°, 4978 m. **(F)** Thick white to light orange bacterial mat nearly covering sheet flow at 18.70751°, –155.18401°, 4981 m.

fissures have been identified, as occur on the northwest and north flanks of Mauna Loa (Wanless et al., 2006). The summit platform has three collapse pits in the southern part and is rimmed by a series of low cones/shields. The eastern portion of the summit platform and southeastern portion of the north rift ends at a steep cliff. This amphitheater has an upper rugged zone with spurs perpendicular to the upper break-in-slope and a smooth lower slope. A similar structure occurs on the west side of the southern summit platform, although the break-in-slope is not as steep as on the east side, nor the lower slope as smooth. Two additional amphitheaters occur on the east and west edges of the middle south rift, leaving a narrow ridge defining the rift zone. The lower slopes of both these amphitheaters are not as smooth as the others, nor are their upper slopes as steep. A NE-SW-oriented ridge, named the Shinkai Ridge (**Figure 8**), is located to the southeast of Lō'ihi. It consists of lava flows, as observed during *Shinkai* submersible dives.

The north rift zone bifurcates into two ridges near ~1600 m depth where it appears to be built on top of the smooth Punalu'u slide structure (**Figure 2**; Moore and Chadwick, 1995). One rift is oriented north-south and the other roughly northeast-southwest. They intersect the south rift zone near West Pit (**Figure 2**). Such bifurcation of distal rift zones is also seen elsewhere in the Hawaiian Islands, such as the Haleakalā east rift zone (Smith et al., 2002). The distal south rift becomes ill-defined below ~3500 m depth and resembles the distal end of Puna Ridge on Kīlauea (Clague et al., 1993, 1995) with lobes radiating from the inferred rift axis.

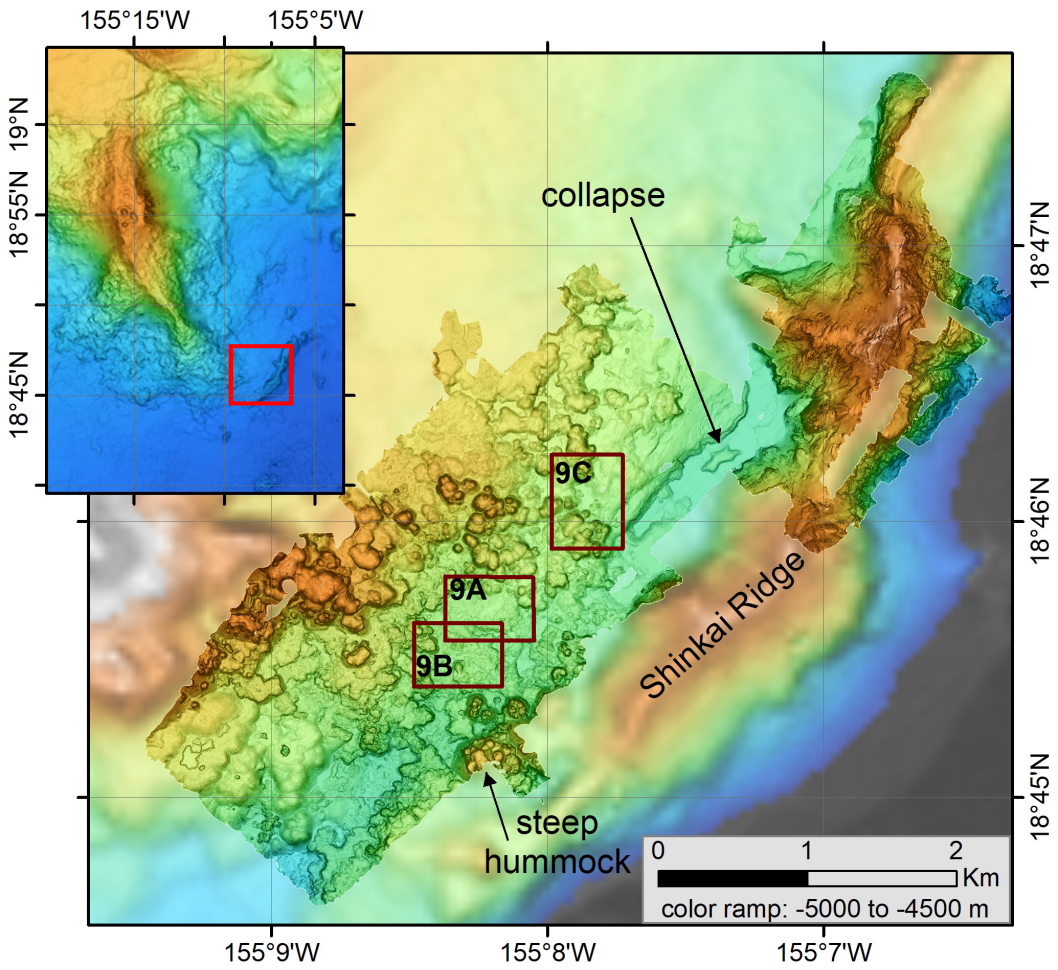

FIGURE 8 | AUV *Sentry* bathymetry showing the combined map of missions 266 and 270 at Shinkai Deep hydrothermal site **(near center)** and during missions 267 and 269 at Shinkai Ridge **(upper right)**. Boxes identify maps shown at higher resolution in **Figure 9**. The data are gridded at 2 m.

Backscatter Characteristics

Holcomb et al. (1988), from the GLORIA side-scan sonar surveys, identified a region of high backscatter around the base of Lō'ihi Seamount that they inferred to be young, far-traveled, lava flows. The GLORIA data were poorly located and the outline of the flows they drew does not coincide with the new bathymetry. The flow boundary was redrawn (**Figure 2**) using mosaicked backscatter data from the GPS-navigated JAMSTEC cruises, guided by the outline of Holcomb et al. (1988). A SeaMark II sidescan survey of the south side of Hawaii Island (Fryer et al., 1987; Smith et al., 1994) also shows high-backscatter lava flows at the base of Lō'ihi Seamount and was also used in redrawing the outline of the high-backscatter flows (**Figure 2**). In many places the high-backscatter areas from the SeaBeam and SeaMark II data are not as clear as from the GLORIA imagery, suggesting that some of these flows are buried under sediment that the GLORIA sonar penetrated more deeply than either the SeaMark II or the SeaBeam sonars. Elsewhere around the Hawai'ian Island chain, GLORIA penetrated at least three meters of sediment (Clague et al., 2002), so some of the high-backscatter flows may not be recently emplaced. Some of these flows are located up to ∼20 km from the summit or south rift zone.

High-Resolution Bathymetry of the Summit Caldera Complex

The summit of Lō'ihi has three pit craters between 0.8 and 1.2 km across: East Pit (EP, **Figure 10**), West Pit (WP) and Pele's Pit (PP) and four smaller pit craters (**Figure 10**). All have steep inward facing crater scarps. The uppermost south rift has two adjoined < 100-m diameter pit craters (P-A and P-B, **Figure 10** and **Table 1**) that are ∼40 m deep. These two small pit craters are aligned north-northwest with a low cone (C2, **Figure 10**), Pele'e Pit, and West Pit; this trend defines the orientation of the upper south rift zone.

The southern summit displays a complex series of structures, most of which are nested collapse structures with inward-facing scarps (**Figure 10**). West Pit and Pele's Pit have numerous re-entrants and spurs extending inward from the rim of the pits (**Figure 4**). The first scarp outside West Pit (R4, **Figure 10** and **Table 1**) and concentric with the pit, has outward-facing scarps

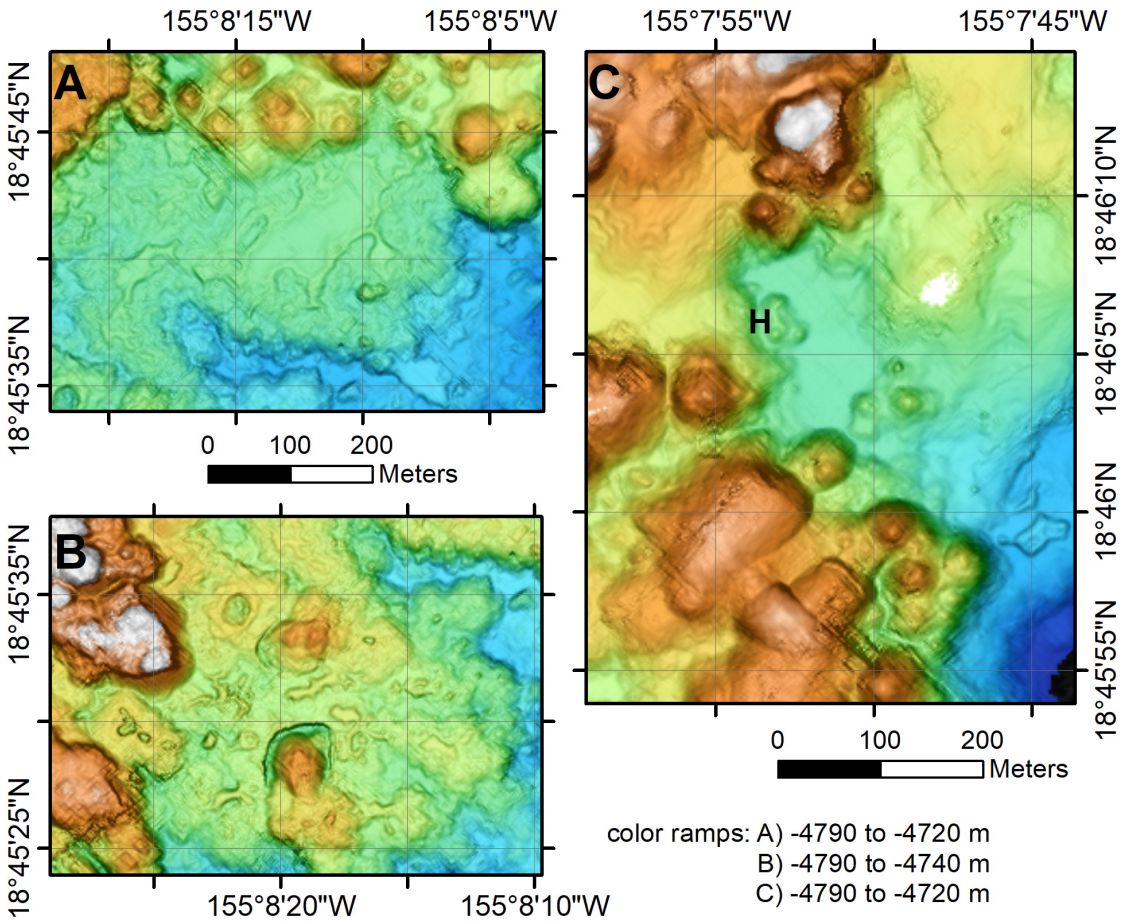

FIGURE 9 | Close-up of AUV *Sentry* bathymetry. The data are gridded at 2 m. **(A)** A channelized flow adjacent to the Shinkai Ridge. **(B)** A small pillow cone crosscutting the margin of a small collapse pit near the Shinkai Deep site. **(A,B)** Are at the same scale. **(C)** The Shinkai Deep hydrothermal site (marked by H) is located on the edge of a sediment-covered channelized flow adjacent to a hummocky flow ~50 m across. Extent of maps are shown by boxes on **Figure 8**.

more than 100 m high that bound an uplifted block. This is the only outward-facing scarp on the summit. East Pit (**Figure 10** and **Table 1**) is also nested within a more extensive series of inward-facing scarps that encircle both East and West Pits. High-flux lava flows with channels and shallow collapses cover the summit platform E and NE of East Pit (one is labeled "flow" on **Figure 10**), but were trapped inside the inward facing scarps (R1, **Figure 10**) that define part of the R1 summit caldera. These flows, and others north of North Pit are buried by volcaniclastic sediment (Clague et al., 2003; Clague, 2009; Schipper and White, 2010). Volcaniclastic sediment up to 11-m thick crop out at the tops of some of the outer caldera-bounding scarps (V, **Figure 10**), but were not observed on submersible dives inside the outermost caldera-bounding scarps.

The northern part of the summit platform was not mapped using AUV *Sentry*, but the deep-tow (**Figure 3**) and EM302 data show two shallow pit craters (P-C and P-D, **Figure 10** and **Table 1**) with the southern P-C about 600 m across and 103 m deep and the northern P-D about 450 m across and 91 m deep. They are aligned north-south with West Pit and the eastern of the two north rift zones and a cone (C1, **Figure 10**).

High-Resolution Bathymetry of Constructional Volcanic Features

Lō'ihi is characterized by having few identifiable constructional cones or shields, at the resolution of ship bathymetry. Most upper south rift eruptive vents consist of ramparts and haystack-like vents. The ramparts appear in the ship bathymetry as linear rift-parallel ridges. The summit and rifts generally have cones below the resolution of shipboard bathymetry. The constructional flanks of the rift zones consist of overlapping lobes of lava, presumably emplaced during fissure eruptions (**Figure 2**). The flanks of the summit are lacking overlapping lobes of flows, and instead are cut by steep cliffs to the E and W of the summit platform, which are discernable in ship bathymetry (**Figure 2**). Collapse structures truncate at least five pre-existing lava shields (S1–S5, **Figure 10**) whose remnants are at the S and N ends of East Pit, W of West Pit and surrounding Pele's Pit (**Figure 10** and **Table 1**). The two largest cones on the seamount occur near the south end of the south rift zone (**Figure 6A**) and are most likely monogenic. These two cones have smooth lower and middle slopes at the resolution of the *Sentry* data (**Figure 6A**) and summits of steeper knobby terrain. The southern cone is elongate

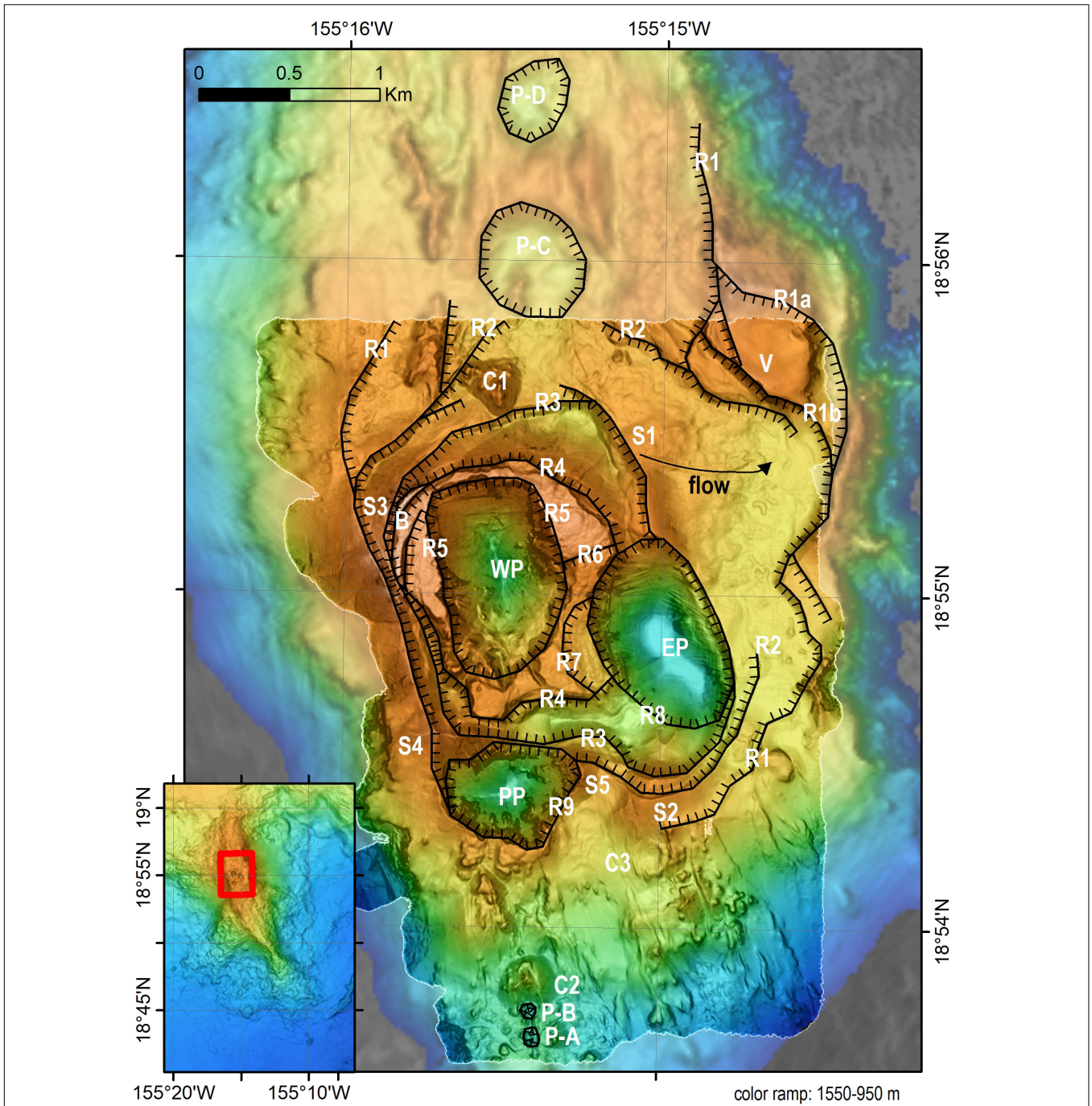

FIGURE 10 | Summit bathymetry with interpretive overlay of caldera and pit crater bounding scarps. *Sentry* data in foreground with Simrad EM302 data behind. Hatchures indicate down-thrown side of caldera or pit crater bounding scarps or ring faults R1 (oldest) to R9 (youngest). Exact sequence of formation for some collapse events cannot be determined. P-A to P-D are pit craters described in the text and in **Table 1**. EP is East Pit, WP is West Pit, PP is Pele's Pit, C1 to C3 indicate two cones described in the text, S1 to S5 indicate the remnants of five lava shields, B indicates 1996 basaltic breccia, and V indicates volcaniclastic sediment 5–11 m thick (Clague et al., 2003; Schipper and White, 2010) with a basal date of ~5900 years (Clague, 2009). Arrow labeled "flow" indicates direction of channelized flow from S1 to the east.

in a NE-SW orientation that is not parallel to the underlying rift orientation. Other constructional cones occur on the summit platform and upper south rift zone (C1 and C2, **Figure 10**), but are small compared to other submarine cones in Hawaii and lack the flat tops commonly observed (Clague et al., 2000). A low cone with a large-diameter crater (C3, **Figure 10**) is located S of East Pit and low shield S2 and ~1 km E of the south rift zone. No other similar cones were identified.

TABLE 1 | Lō'ihi pit craters.

Feature	Diameter (m)	Long direction	Depth (m)
West pit	1100 × 700	N-S	299
East pit	1050 × 650	NW-SE	300
Pele's pit	700 × 500	E-W	332
P-A	100	Circular	41
P-B	90	Circular	40
P-C	580 × 610	NW-SE	103
P-D	480 × 365	NE-SW	91

Depth is from highest point on rim to deepest point.

High-Resolution Bathymetry of the FeMO Hydrothermal Site

The same AUV *Sentry* surveys that mapped the two smooth cones on the deep south rift zone also mapped a series of low hummocky lava flows that entered the mapped region from the northwest and stagnated just west of the southeastern smooth cone (**Figure 5B**). These hummocky flows display numerous small collapse structures indicative of molten interiors (see description of similar flows on Axial Seamount in Clague et al., 2017). Rapidly emplaced flows with channels and shallow drainout depressions appear to start at the margins of the thicker hummocky flows (**Figures 6B,C**). The hummocky mounds generally increase in depth along the flow (indicated by arrows on **Figure 5B**). In contrast, the easternmost mound is shallower than the mound just to the west from which it was fed. These lava flows host the FeMO low-temperature hydrothermal vents (Glazer and Rouxel, 2009). These hummocky and channelized flows (**Figure 7**) have very thin sediment, except in the vicinity of discharging low-temperature hydrothermal fluids (**Figures 7E,F**).

High-Resolution Bathymetry of the Shinkai Deep and Ridge Hydrothermal Sites

The map of the Shinkai Deep and Ridge on the south-southeast flank of Lō'ihi (**Figure 8**) illustrates a number of lava morphologies. Much of the mapped area is constructed of single steep-sided hummocky pillow flows lacking small collapse pits. The hummocks near the south-central part of the map (near 155°8′W, 18°45.2′N) are near the base of the northeast-southwest trending Shinkai Ridge and rise to shallower depths than the flows to the northwest that fed them. Many of these steep-sided flows, especially those in the northwestern part of the map, have smooth slopes around them or at their bases. A very few of the hummocky flows have small collapse pits indicative of molten cores (Clague et al., 2017). The central part of **Figure 8** shows some high-flux channelized flows which are characterized by subdued topography (**Figure 9A**). A 50-m diameter hummock (south-central **Figure 9B**) is surrounded by a shallow collapse structure in the surrounding channelized flow, indicating that the hummock was built on top of the channelized flow before it had solidified so that both the hummock and upper crust of the channelized flow could subside when magma was drained from within the channelized flow. A 50–70 m diameter low cone with a 30–50 m-diameter crater is located a few hundred m to the north-northwest. The Shinkai Deep hydrothermal vent site (H, **Figure 9C**) is located at the edge of hummocky flows that overlie an older low-relief remnant of a channelized flow. Dive observations from the *Shinkai* submersible indicate that the flows are covered by thick sediment and are therefore inferred to be old.

AUV *Sentry* mapping of Shinkai Ridge is restricted to the northeastern part (**Figure 8**), but the ridge has no identifiable constructional volcanic characteristics. A channelized flow ponded at the northwestern base of the ridge and inflated, forming several large collapsed areas as lava drained from under the crust (labeled on **Figure 8** and in southeast corner of **Figure 9C**). This lava flow marks the southeastern edge of the high-backscatter flows (**Figure 2**) originally mapped by Holcomb et al. (1988), although the Shinkai Ridge also has high backscatter due to its steepness.

DISCUSSION

Structure and Evolution of the Summit

The relatively flat summit plateau has had a complex evolution consisting of multiple constructional and collapse structures that were unrecognized based on lower resolution surveys. These constructional and collapse structures have significant implications for defining the magma storage system within Lō'ihi Seamount. We use the nomenclature for calderas from Cole et al. (2005), which follows closely from Lipman (2000). The outermost inward-facing scarps are ring or caldera faults (R1, **Figure 10**) that define a caldera ∼ 3 km across. It is therefore about half the average ∼6 km diameter for basaltic calderas globally (Gudmundsson, 2008) and also about half the size of the summit calderas on Kīlauea and Mauna Loa Volcanoes on Hawaii (**Figure 2**). The arcuate inward-facing ring fault on the northeast margin includes several steps (R1a and R1b, **Figure 10**) that may represent slumped portions of caldera walls, or two similar sized calderas. The base of an 11-m thick sequence of volcaniclastic sediment (V, **Figure 10**) exposed in the northeastern R1 scarp is 5900 years old (Clague, 2009), and formed before or during the collapse of the earliest and largest of the recognized calderas.

These R1 scarps define parts of a caldera that extended to the south, west and north margins of the summit, but portions of the northern, southern and eastern scarps are missing. The southern and northern bounding caldera scarps have probably been buried by subsequent lava whereas some of the western boundary and some parts of the eastern bounding fault scarps were likely removed during younger outward-directed landslides as discussed below.

Within this outermost inward-facing caldera scarp, four nested caldera scarps cut low lava shields and encircle West Pit. The outer two caldera scarps (R2 and R3, **Figure 10**) are inward-facing, but the next (R4, **Figure 10**) is a steeply dipping outward-facing fault scarp that bounds an uplifted block and suggests a period of resurgence prior to formation of the final inward-facing pit crater scarp (R5, **Figure 10**) that bounds West Pit. The collapses have progressively smaller diameters with the R2 caldera being 2.5 km in diameter, the R3 caldera 2 × 1.5 km,

the R4 resurgent block ∼1.3 km in diameter, and the R5 pit crater (West Pit) 1 × 0.7 km. West Pit, as well as the younger East Pit and the youngest Pele's Pit are similar to other pit craters in being < ∼1 km across (Gudmundsson, 2008). The progressive decrease in dimensions of these collapse and resurgent features suggest a shoaling of the magma reservoir beneath them (e.g., Acocella et al., 2000, 2001; Kusumoto and Takemura, 2005), while maintaining the general location of the reservoir beneath West Pit. The periods of collapse generally followed periods of summit eruptions that formed low lava shields that the collapses partially destroyed.

Based on cross cutting relations, three collapses (Okubo and Martel, 1998) centered on East Pit formed R6, R7, and R8 next (**Figure 10**). The final pit crater collapse event was the formation of Pele's Pit in 1996 defined by R9 (**Figure 10**; Lō'ihi Science Team, 1997; Davis and Clague, 1998). Pele's Pit is located at the former location of a lava shield constructed of an evolved alkalic basalt with 5.17 wt% MgO (sample 1804-19 in Garcia et al., 1993). The 1996 lava breccia (B, **Figure 10**) is a tholeiitic basalt with an average 6.85 wt% MgO (Garcia et al., 1998), so Pele's Pit did not form from the draining of alkalic magma stored beneath the shield. The serrated rims of West and Pele's Pits formed by numerous small landslides (each 50 to a few 100 m wide) into the pit. East Pit shows similar features on the west side, but the eastern and southern margins are smooth, and resemble Halema'uma'u pit crater on Kīlauea prior to the 2018 collapse of Kīlauea's summit from May to early August 2018 (Neal et al., 2019).

The timing of formation of pit craters P-A to P-D (**Figure 10**) is largely unknown, although P-C and P-D may well be located within the original caldera bounded by R1 caldera scarps. If this is the case, then the R1 caldera had an elongate N-S orientation and was about 2.5 by 4.5 km in size. An elongate caldera would be expected in an extensional setting (Acocella et al., 2004). Based on observed changes at Kīlauea's summit in May-August 2018 (Neal et al., 2019), several of these collapse structures may have formed at the same time or in sequence during a single period of summit collapse.

The period of resurgence indicated by outward-facing scarp R4 is the first known from the Hawaiian Islands, but is known from other volcanoes such as Pantelleria and Ischia Island near Naples (Tibaldi and Vezzoli, 1998; Acocella and Funiciello, 1999; Acocella et al., 2001; Molin et al., 2003). The outward-facing scarps indicate uplift of a resurgent block. The diameter of the block should be roughly equal to the depth to the top of the magma reservoir (Acocella et al., 2001), in this case, ∼1.3 km. The northwestern side of the resurgent block is the shallowest part of Lō'ihi's summit at 986 m depth, and the block is tilted about 6.5° with the northwestern edge uplifted relative to the southeastern edge.

Collapses to form calderas or pit craters on basaltic volcanoes, for example, have been documented previously in 1968 at Fernandina in the Galapagos Islands (Simkin and Howard, 1970; Filson et al., 1973; Munro and Rowland, 1996; Howard, 2010), in 2000 at Miyakejima in Japan (Kumagai et al., 2001), in 2007 at Piton de La Fournaise volcano on Reunion Island (Michon et al., 2007, 2009; Peltier et al., 2009), and in 2018 at Kīlauea Volcano (Neal et al., 2019). In each case the events were piston cylinder events, with incremental downdropping of the piston over periods lasting from 1 day (Piton de La Fournaise in 2007) to 77 days (Kīlauea in 2018). The calderas and pit craters on the summit of Lō'ihi probably formed by a similar mechanism over similar time periods.

The sequence of collapse and one resurgent block confirm that Lō'ihi Seamount has had a crustal magma reservoir only one to a few km below the surface for much of the past 5900 years. This inference contrasts with prior interpretation that the magma reservoir was at 8–9 km depth, which was based on petrologic arguments for the 1996 glassy breccia samples (Garcia et al., 1998, and summarized in Garcia et al., 2006). The difference might be reconciled by having two magma reservoirs, one within or at the base of the underlying ocean crust as previously proposed (Clague, 1988; Garcia et al., 2006) and a second, much shallower reservoir that underlies the caldera and pit crater structures by just 1–2 km. That residence in the shallow reservoir was not identified petrologically is consistent with only brief residence of the 1996 magma in the shallowest reservoir, which in turn is consistent with its inferred small diameter and volume. The presence of a shallow sub-caldera magma reservoir at Lō'ihi Seamount establishes the early development of magma storage in Hawaiian volcanoes.

Rift Eruptions

Caldera formation on basaltic volcanoes is commonly inferred to be triggered by rapid magma withdrawal from the reservoir beneath the edifice (e.g., Pinel and Jaupart, 2005; Geshi et al., 2014) and observed at Kīlauea in 2018 (Neal et al., 2019). This withdrawal of magma from beneath the summits was caused by flank eruptions coinciding with recent caldera and pit-crater forming eruptions discussed above, and formation of calderas and pit craters at Lō'ihi was probably triggered by the same mechanism.

Immediately following the 1996 collapse of Pele's Pit, six samples from a glassy breccia dated using ^{210}Po-^{210}Pb (labeled B on **Figure 10**) were collected west and northwest of West Pit during *Pisces V* submersible dives 286 and 287 (Garcia et al., 1998), but no downrift lava flows were located. The glassy breccia fragments were erupted in 1996, most likely during brief activity of one of the many caldera-bounding faults nearby, as no eruption appears to have occurred within West Pit. Several additional dives within the 2000 m depth range of the *Pisces V* submersible were used in 1998 to search the south rift zone for young lavas that might be the "missing flow," but no young flows were identified. Several sites of low-temperature fluid venting were found (Wheat et al., 2000), but the underlying and nearby flows were not young.

The deep south rift extension near the FeMO hydrothermal site (**Figure 5**) is characterized by channelized to hummocky flows with molten cores and drainbacks that are similar to flows erupted on Axial Seamount on the Juan de Fuca spreading center in 2015 (Clague et al., 2017). Likewise, similar complex advance of inflated hummocky flows was described in Clague et al. (2017) for part of the 2015 lava flow on Axial Seamount. Flows with this morphology form during moderate effusion-rate eruptions

lasting for weeks or longer. The flows surrounding the FeMO hydrothermal site are also almost free of non-hydrothermal sediment and have abundant low-temperature fluid venting that has deposited abundant yellow-orange hydrothermal sediment and supports active bacterial mats. These are characteristics seen on historical Axial Seamount lava flows (see e.g., Chadwick et al., 2013, Clague et al., 2017) where they have been observed for more than a decade following flow emplacement. Unfortunately, the lavas near the FeMO site on Lō'ihi have not been sampled, but we suspect that these flows were erupted in 1996 and that their emplacement on the deep rift zone led to the collapse of Pele's Pit at the summit.

The large flows that surround the base of Lō'ihi Seamount (Holcomb et al., 1988) appear to have erupted from the south rift axis and flowed long distances down relatively gentle slopes. The large volumes of these flows make them good candidates to have triggered summit collapses on Lō'ihi, but none have been sampled nor their ages determined to correlate with the summit caldera-forming events.

Formation of Volcanic Landforms

Lō'ihi Seamount is characterized by small-diameter cones (generally < 300 m in basal diameter) probably of monogenetic origin and linear spatter ramparts that are indicative of brief, small-volume eruptions. This is especially true for the summit of Lō'ihi where cones are very rare. As volcanoes grow and evolve, small cones and ramparts are supplanted by longer steadier eruptions that construct larger volume volcanic landforms such as shields or flat-topped cones (Clague et al., 2000).

The two largest cones on Lō'ihi Seamount (**Figure 6A**) are unusual in having very smooth flanks that elsewhere have been shown to consist of basaltic pillow talus deposited at the base of steep-sided hummocky pillow mounds. Such deposits formed during the 1996 North Gorda eruption (Paduan et al., 2014) and the 2011 Axial eruption on the distal south rift zone (Clague et al., 2017) and are indicative of very low eruption rate pillow mounds with the talus fragments forming during the eruption as pillows cascade over near-vertical scarps. Cones as large as the two near the base of the south rift on Lō'ihi likely took weeks to months of low-eruption rate activity to form. Many of the steep-sided hummocky flows around the Shinkai Deep (**Figure 9**) show similar smooth lower slopes and are also inferred to consist of talus formed during growth of the steep-sided flows.

Other lava flows, such as those on the summit platform east of East Pit are channelized flows that are inferred to have erupted at high effusion rates during brief eruptions as documented for several historical eruptions on Axial Volcano (Chadwick et al., 2013; Clague et al., 2017).

Landslides

The flank landslides (Fornari et al., 1988; Moore et al., 1989) on the east side of the summit (**Figure 2**) cut and removed part of the outermost caldera-bounding faults and therefore occurred or at least enlarged the headwall regions of the slides since formation of the largest outer summit caldera, inferred to be ∼5900 years ago (Clague, 2009). We think it most likely that the landslide headwalls have simply stepped toward the summit in that time period. These are the youngest of the landslides around the Hawaiian Islands that modify entire volcanoes (Moore et al., 1989).

The Shinkai Ridge may be a detached slide block that originated either on the east flank of Lō'ihi near the summit or from the southern margin of the Punaluu landslide from Mauna Loa prior to formation of Lō'ihi Seamount. JAMSTEC dive K96 of the ROV *Kaiko* recovered 5 picrite and olivine basalt samples and one mudstone from the ridge in 1998 and one volcanic breccia that was analyzed; it has a composition similar to Lō'ihi Seamount lavas, and distinct from Mauna Loa lavas, as expected if it were a block of the Punalu'u slide (Coombs et al., 2004). The block most likely originated from the east flank of Lō'ihi and was emplaced near the southern end of Lō'ihi as a landslide block. To arrive at its present location, the block would have undergone a clockwise rotation of nearly 90° and slid, as a coherent block, about 45 km to the south-southeast.

The new mapping data provide an opportunity, beyond the scope of this paper, to evaluate what features were sampled during the many prior dives and dredges. Complete high-resolution mapping of the rest of the summit and the north and south rift zones would reveal more of the complex history of Lō'ihi Seamount. A new generation of submersible or ROV dives done with improved navigation would allow for construction of a detailed structural and magmatic evolution of Lō'ihi.

CONCLUSION

The new high-resolution summit bathymetry at Lō'ihi Seamount shows a nested series of eight caldera and pit crater collapses events, uplift of one resurgent block, and eruptions that formed at least five low lava shields. The oldest and largest caldera-bounding faults enclose almost the entire summit plateau. Resurgence that uplifted a fault-bounded block > 100 m was the fourth tectonic event at the summit and followed three caldera collapse events and preceded formation of five pit craters. The most recent collapse formed Pele's Pit in 1996. Each of the nine mapped collapse or resurgent structures indicates the presence of a shallow crustal magma chamber, ranging from depths between 1 km and perhaps 2 km. Shallow sub-caldera magma reservoirs therefore exist during the late pre-shield stage of Hawaiian volcanism. The structural history of caldera and pit crater formation on Hawaiian volcanoes, other basaltic volcanoes, and volcanoes in general, provides a framework for understanding the evolution, size, and depth of their magma storage systems.

The summit collapse events, including the last one in 1996, were probably triggered by draining the crustal magma reservoir to supply magma to eruptions on the deep south rift zone. Extensive young lavas that host the FeMO hydrothermal vent field (**Figure 6D**) at ∼18°42.2′N, 155°10.55′W, likely erupted in 1996 and the low-temperature venting of heat extracted by fluids circulated in the thick lava field. The Shinkai Deep hydrothermal site is located among older sediment-covered steep-sided hummocky flows. These steep-sided mounds produced talus during their formation as advancing pillows broke

off and tumbled downslope. Two smooth-sloped cones on the deep south rift near the FeMO hydrothermal site formed by a similar process.

The summit and rift zones of Lō'ihi have been modified by landslides, with the youngest landslide activity occurring after formation of the oldest summit caldera about 5900 years ago. Most of the landslide activity produces smooth talus slopes below steep headwalls, but the Shinkai Ridge near the southern base of Lō'ihi is most likely a coherent landslide block that originated on the east flank of the volcano.

DATA AVAILABILITY

The multibeam datasets processed for this study can be found in the IDEA seafloor bathymetry archives.

AUTHOR CONTRIBUTIONS

CM and BG were chief scientists on the two cruises that collected the AUV *Sentry* data. DY designed the surveys and did initial processing of the data during the 2014 cruise. DWC did the initial processing of the HUGO cable-route survey and assisted and advised JP and DAC on processing the AUV bathymetric data. JP did the extensive MB-System processing of the AUV data, constructed most of the figures, and contributed to editing the manuscript. DAC assisted with editing and processing the AUV data and wrote the manuscript.

FUNDING

Funding for the collection of the data was provided by the National Science Foundation OCE1155756 to CM and the Schmidt Ocean Institute to BG. Support for DC and JP to process the data and write the manuscript was provided by a grant from the David and Lucile Packard Foundation to MBARI.

ACKNOWLEDGMENTS

The 2013 AUV *Sentry* surveys were conducted off the R/V *Kilo Moana* and the 2014 surveys were conducted off the R/V *Falkor*. We would like to thank the crews of both ships and the AUV *Sentry* team from Woods Hole Oceanographic Institution, especially team leader Carl Kaiser in 2013, for their assistance at sea.

REFERENCES

Acocella, V., Cifelli, F., and Funiciello, R. (2000). Analogue models of collapse calderas and resurgent domes. *J. Volcanol. Geotherm. Res.* 104, 81–96. doi: 10.1016/S0377-0273(00)00201-8

Acocella, V., Cifelli, F., and Funiciello, R. (2001). The control of overburden thickness on resurgent domes: insights from analogue models. *J. Volcanol. Geotherm. Res.* 111, 137–153. doi: 10.1016/S0377-0273(01)00224-4

Acocella, V., and Funiciello, R. (1999). The interaction between regional and local tectonics during resurgent doming: the case of the islands of Ischia, Italy. *J. Volcanol. Geothermal. Res.* 88, 109–123. doi: 10.1016/S0377-0273(98)00109-7

Acocella, V., Funiciello, R., Marotta, E., Orsi, G., and de Vita, S. (2004). The role of extensional structures on experimental calderas and resurgence. *J. Volcanol. Geotherm. Res.* 129, 199–217. doi: 10.1016/S0377-0273(03)00240-3

Bryan, C., and Cooper, P. (1995). Ocean-bottom seismometer observations of seismic activity at Loihi Seamount, Hawaii. *Mar. Geophys. Res.* 17, 485–501. doi: 10.1007/BF01204340

Caplan-Auerbach, J., and Duennebier, F. K. (2001a). Seismicity and velocity structure of Loihi Seamount from the 1996 earthquake swarm. *Bull. Seismo. Soc. Am.* 91, 178–190. doi: 10.1785/0119990170

Caplan-Auerbach, J., and Duennebier, F. K. (2001b). Seismic and acoustic signals detected at Loihi Seamount by the Hawaii Undersea Geo-Observatory. *Geochem. Geophys. Geosyst.* 2:1024. doi: 10.1029/2000GC000113

Caress, D. W., and Chayes, D. N. (2011). *MB-System: Mapping the Seafloor*. Available at: http://www.mbari.org/data/mbsystem

Chadwick, W. W. Jr., Clague, D. A., Embley, R. W., Perfit, M. R., Butterfield, D. A., Caress, D. W., et al. (2013). The 1998 eruption of Axial Seamount: new insights on submarine lava flow emplacement from high-resolution mapping. *Geochem. Geophys. Geosyst.* 14, 3939–3968. doi: 10.1002/ggge.20202

Chadwick, W. W. Jr., Smith, J. R., Moore, J. G., and Fox, C. (1993). *Bathymetry of the South Flank of Kilauea Volcano, Hawaii*. Reston, VA: U.S. Geological Survey.

Clague, D. A. (1988). Petrology of ultramafic xenoliths from Loihi Seamount, Hawaii. *J. Petrol.* 29, 1161–1186. doi: 10.1093/petrology/29.6.1161

Clague, D. A. (2009). Accumulation rates of volcaniclastic sediment on Loihi Seamount, Hawaii. *Bull. Volcanol.* 71, 705–710. doi: 10.1007/s00445-009-0281-y

Clague, D. A., Batiza, R., Head, J., and Davis, A. S. (2003). "Pyroclastic and hydroclastic deposits on Loihi Seamount, Hawaii," in *Explosive Subaequeous Volcanism, American Geophysical Union Monograph*, Vol. 140, eds J. D. L. White, J. L. Smellie, and D. A. Clague (Washington, DC: American Geophysical Union), 73–95. doi: 10.1029/140GM05

Clague, D. A., and Dalrymple, G. B. (1987). "The hawaiian-emperor volcanic chain," in *Volcanism in Hawaii, US Geological Survery Professional Paper*, Vol. 1350, eds R. W. Decker, T. L. Wright, and P. H. Stauffer (Washington, DC: United States Government Publishing Office), 5–54.

Clague, D. A., Hon, K. A., Anderson, J. L., Chadwick, W. W. Jr., and Fox, C. G. (1993). *Bathymetry of Puna Ridge, Kilauea Volcano, Hawaii*. Reston, VA: United States Geological Survey Miscellaneous Field Map MF-2237.

Clague, D. A., Moore, J. G., Dixon, J. E., and Friesen, W. B. (1995). Petrology of submarine lavas from Kilauea's Puna Ridge, Hawaii. *J. Petrol.* 36, 299–349. doi: 10.1093/petrology/36.2.299

Clague, D. A., Moore, J. G., and Reynolds, J. R. (2000). Formation of submarine flat-topped volcanic cones in Hawaii. *Bull. Volcanol.* 62, 214–233. doi: 10.1007/s004450000088

Clague, D. A., Paduan, J. B., Caress, D. W., Chadwick, W. W. Jr., Le Saout, M., Dreyer, B., et al. (2017). High-resolution AUV mapping and targeted ROV observations of three historical lava flows at Axial Seamount. *Oceanography* 30, 82–99. doi: 10.5670/oceanog.2017.426

Clague, D. A., Uto, K., Satake, K., and Davis, A. S. (2002). "Eruption style and flow emplacement in the submarine North Arch Volcanic Field, Hawaii," in *Hawaiian Volcanoes: Deep Underwater Perspectives*, Vol. 128, eds E. Takahashi, P. W. Lipman, M. O. Garcia, J. Naka, and S. Aramaki (Washington, DC: American Geophysical Union), 65–84. doi: 10.1029/GM128p0065

Cole, J. W., Milner, D. M., and Spinks, K. D. (2005). Calderas and caldera structures: a review. *Earth Sci. Rev.* 69, 1–26. doi: 10.1016/j.earscirev.2004.06.004

Coombs, M. L., Sisson, T. W., and Lipman, P. W. (2004). *Major-Element, S, and Cl Compositions of Submarine Kilauea Glasses Collected During the 1998–2002 JAMSTEC Hawaii cruises*. Reston, VA: U.S. Geological Survey 2004–1378,

Davis, A. S., and Clague, D. A. (1998). Changes in the hydrothermal system at Loihi Seamount after the formation of Pele's pit in 1996. *Geology* 26, 399–402. doi: 10.1130/0091-7613(1998)026<0399:CITHSA>2.3.CO;2

Davis, A. S., Clague, D. A., Zierenberg, R. A., Wheat, C. G., and Cousens, B. L. (2003). Sulfide formation related to changes in the hydrothermal system on Loihi Seamount, Hawaii, following the seismic event in 1996. *Can. Min.* 41, 457–472. doi: 10.2113/gscanmin.41.2.457

De Carlo, E. H., McMurtry, G. M., and Yeh, H. W. (1983). Geochemistry of hydrothermal deposits from Loihi submarine volcano, Hawaii. *Earth Planet. Sci. Lett.* 66, 438–449. doi: 10.1016/0012-821X(83)90157-7

Duennebier, F. K., Harris, D., Jolly, J., Caplan-Auerbach, J., Jordan, R., Copson, D., et al. (2002). HUGO: the Hawaii Undersea Geo-Observatory. *IEEE J. Ocean Eng.* 2, 218–227. doi: 10.1109/JOE.2002.1002476

Eakins, B. W., Robinson, J. E., Kanamatsu, T., Naka, J., Smith, J. R., Takahashi, E., et al. (2004). *Hawaii's Volcanoes Revealed*. Reston, VA: U.S. Geological Survey.

Edwards, K. J., Glazer, B. T., Rouxel, O. J., Bach, W., Emerson, D., Davis, R. E., et al. (2011). Ultra-diffuse hydrothermal venting supports Fe-Oxidizing bacteria and massive umber deposition at 5000 m off Hawaii. *ISME J.* 5, 1748–1758. doi: 10.1038/ismej.2011.48

Emery, K. O. (1955). Submarine topography south of Hawaii. *Pac. Sci.* 9, 286–291.

Filson, J., Simkin, T., and Leu, L. K. (1973). Sesimicity of a caldera collapse: Galapagos Islands 1968. *J. Geophys. Res.* 78, 8591–8622. doi: 10.1029/JB078i035p08591

Fornari, D. J., Garcia, M. O., Tyce, R. C., and Gallo, D. G. (1988). Morphology and structure of Loihi seamount based on seabeam sonar mapping. *J. Geophys. Res.* 93, 15227–15238. doi: 10.1029/JB093iB12p15227

Frey, F. A., and Clague, D. A. (1983). Geochemistry of diverse basalt types from Loihi Seamount, Hawaii: petrogenetic implications. *Earth Planet. Sci. Lett.* 66, 337–355. doi: 10.1016/0012-821X(83)90150-4

Fryer, P., Matsumoto, H., Duennebier, F., Cooper, P., Kellogg, J., Garcia, M., et al. (1987). Loihi Seamount: a reconnaissance Sea MARC II survey. *Geol. Soc. Am. Trans.* 19:380.

Garcia, M. O., Caplan-Auerbach, J., De Carlo, E. H., Kurz, M. D., and Becker, N. (2006). Geology, geochemistry, and earthquake history of Loihi Seamount, Hawaii's youngest volcano. *Chem. Erde* 66, 81–108. doi: 10.1016/j.chemer.2005.09.002

Garcia, M. O., Graham, D. W., Muenow, D. W., Spencer, K., Rubin, K. H., Norman, M. D., et al. (1998). Petrology and geochronology of basalt breccia from the 1996 earthquake swarm of Loihi Seamount, Hawaii: magmatic history of its 1996 eruption. *Bull. Volcanol.* 59, 577–592. doi: 10.1007/s004450050211

Garcia, M. O., Irving, A. J., Jorgenson, B. A., Mahoney, J. J., and Ito, E. (1993). An evaluation of temporal geochemical evolution of Loihi summit lavas: results from Alvin submersible dives. *J. Geophys. Res.* 98, 537–550. doi: 10.1029/92JB01707

Garcia, M. O., Muenow, D. W., Aggrey, K. E., and O'Neil, J. R. (1989). Major element, volatile, and stable isotope geochemistry of Hawaiian submarine tholeiitic glasses. *J. Geophys. Res.* 94, 10525–10538. doi: 10.1029/JB094iB08p10525

Geshi, N., Ruch, J., and Acocella, V. (2014). Evaluating volumes for magma chambers and magma withdrawal for caldera collapse. *Earth Planet. Sci. Lett.* 396, 107–115. doi: 10.1038/ncomms12295

Glazer, B. T., and Rouxel, O. J. (2009). Redox speciation and distribution within diverse iron-dominated microbial habitats at Loihi Seamount. *Geomicrobiol. J.* 26, 606–622. doi: 10.1080/01490450903263392

Gudmundsson, A. (2008). Magma Chamber geometry, fluid transport, local stresses and rock behavior during caldera formation. *Dev. Volcanol,* 10, 313–349. doi: 10.1016/S1871-644X(07)00008-3

Holcomb, R. T., Moore, J. G., Lipman, P. W., and Belderson, R. H. (1988). Voluminous lava flows from Hawaiian volcanoes. *Geology* 16, 400–404. doi: 10.1130/0091-7613(1988)016<0400:VSLFFH>2.3.CO;2

Holcomb, R. T., and Robinson, J. E. (2004). *Maps of the Hawaiian Islands Exclusive Economic Zone Interpreted from GLORIA Sidescan-Sonar Imagery*. Reston, VA: United States Geological Survey. doi: 10.3133/sim2824

Howard, K. A. (2010). Caldera collapse: perspectives from comparing Galapagos volcanoes, nuclear-test sinks, sandbox models, and volcanoes on Mars. *GSA Today* 20, 4–10. doi: 10.1130/GSATG82A.1

Karl, D. M., Brittain, A. M., and Tilbrook, B. D. (1989). Hydrothermal and microbial processes at Loihi Seamount, a midplate hot-spot volcano. *Deep Sea Res.* 36, 1655–1673. doi: 10.1016/0198-0149(89)90065-4

Karl, D. M., McMurtry, G. M., Malahoff, A., and Garcia, M. O. (1988). Loihi Seamount, Hawaii: a mid-plate volcano with a distinctive hydrothermal system. *Nature* 335, 532–535. doi: 10.1038/335532a0

Klein, F. W. (1982). Earthquakes at Loihi submarine volcano and the Hawaiian hot spot. *J. Geophys. Res.* 87, 7719–7726. doi: 10.1029/JB087iB09p07719

Kumagai, H., Ohminato, T., Nakano, M., Ooi, M., Kubo, A., Unoue, H., et al. (2001). Very long-period seismic signals and caldera formation at Miyake Island. Japan. *Science* 293, 687–690. doi: 10.1126/science.1062136

Kusumoto, S., and Takemura, K. (2005). Caldera geometry determined from depth of the magma chamber. *Earth Planets Space* 57, e17–e20. doi: 10.1186/BF03351879

Lipman, P. W. (2000). in *Calderas, in Encyclopedia of Volcanoes*, ed. H. Sigurdsson (San Diego, CA: Academic Press), 643–662.

Lō'ihi Science Team. (1997). Researchers rapidly respond to submarine activity at Lō'ihi volcano. Hawaii. *EOS Trans. AGU* 78, 229–233. doi: 10.1029/97EO00150

Malahoff, A. (1987). "Geology of the summit of Loihi submarine volcano," in *Volcanism in Hawaii: USGS Professional Paper*, Vol. 1350, eds R. W. Decker, T. L. Wright, and P. H. Stauffer (Reston: VA: United States Geological Survey), 133–144.

Malahoff, A., McMurtry, G. M., Wiltshire, J. C., and Hsueh-Wen, Y. (1982). Geology and chemistry of hydrothermal deposits from active submarine volcano Loihi. Hawaii. *Nature* 298, 234–239. doi: 10.1038/298234a0

MBARI Mapping Team (2000). *Hawaii Multibeam Survey*. Moss Landing, CA: Monterey Bay Aquarium Research Institute

Michon, L., Staudacher, T., Farrazzini, V., and Bachelory, P. (2007). April 2007 collapse of Piton de la Fournaise: a new example of caldera formation. *Geophys. Res Lett.* 34:L21301. doi: 10.1029/2007GL031248

Michon, L., Villeneuve, N., Catry, T., and Merle, O. (2009). How summit calderas collapse on basaltic volcanoes: new insights from the April 2007 caldera collapse of Piton de La Fournaise volcano. *J. Volcanol. Geotherm. Res.* 184, 138–151. doi: 10.1016/j.jvolgeores.2008.11.003

Molin, P., Acocella, V., and Funiciello, R. (2003). Structural, seismic, and hydrothermal features at the border of the active intermittent resurgent block: Ischia Island (Italy). *J. Volcanol. Geotherm. Res.* 121, 65–81. doi: 10.1016/S0377-0273(02)00412-2

Moore, J. G., and Chadwick, W. W. (1995). "Offshore geology of Mauna Loa and adjacent area, Hawaii," in *Mauna Loa Revealed: Structure, Composition, History, and Hazards*, Vol. 92, eds J. M. Rhodes and J. P. Lockwood (Washington, DC: American Geophysical Union), 21–44.

Moore, J. G., Clague, D. A., Holcolm, R., Lipman, P., Normark, W., and Torresan, M. (1989). Prodigious landslides on the Hawaiian ridge. *J. Geophys. Res.* 94, 17465–17484. doi: 10.1029/JB094iB12p17465

Moore, J. G., Clague, D. A., and Normar. k, W. R. (1982). Diverse basalt types from Loihi seamount, Hawaii. *Geology* 10, 88–92. doi: 10.1130/0091-7613(1982)10<88:DBTFLS>2.0.CO;2

Moore, J. G., Normark, W. R., and Lipman, P. W. (1979). "Loihi Seamount – a young submarine Hawaiian volcano," in *Proceedings of the Hawaii Symposium on Intraplate Volcanism and Submarine Volcanism*, Hilo, 127.

Morgan, J. K., Moore, G. F., and Clague, D. A. (2003). Slope failure and volcanic spreading along the submarine south flank of Kilauea volcano, Hawaii. *J. Geophys. Res.* 108:2415. doi: 10.1029/2003JB002411

Munro, D. C., and Rowland, S. K. (1996). Caldera morphology in the western Galapagos and implications for volcano eruptive behavior and mechanisms of caldera formation. *J. Volcanol. Geotherm. Res.* 72, 85–100. doi: 10.1016/0377-0273(95)00076-3

Neal, C. A., Brantley, S. R., Antolik, L., Babb, J. L., Burgess, M., Calles, K., et al. (2019). The 2018 rift eruption and summit collapse of Kilauea Volcano. *Science* 363, 367–374. doi: 10.1126/science.aav7046

Okubo, C. H., and Martel, S. J. (1998). Pit crater formation on Kilauea Volcano, Hawai'i. *J. Volcanol. Geotherm. Res.* 86, 1–18. doi: 10.1016/S0377-0273(98)00070-5

Paduan, J. B., Clague, D. A., and Caress, D. W. (2014). "Constructional talus: built during eruption, not by later tectonism," in *Proceedings of the American Geophysical Union Fall Meeting*, San Francisco, CA.

Peltier, A., Staudacher, T., Bachelery, P., and Cayol, V. (2009). Formation of the April 2007 caldera collapse at Piton de la Fournaise volcano: insights from GPS data. *J. Volcanol. Geotherm. Res.* 184, 152–163. doi: 10.1016/j.jvolgeores.2008.09.009

Pinel, V., and Jaupart, C. (2005). Caldera formation by magma withdrawal from a reservoir beneath a volcanic edifice. *Earth Planet. Sci. Lett.* 230, 273–287. doi: 10.1038/ncomms12295

Schipper, C. I., and White, J. D. L. (2010). No depth limit to hydrovolcanic limu o Pele from Loihi Seamount, Hawaii. *Bull. Volcanol.* 72, 149–164. doi: 10.1007/s00445-009-0315-5

Schipper, C. I., White, J. D. L., and Houghton, B. F. (2011). Textural, geochemical, and volatile evidence for a Strombolian sequence at Loihi Seamount, Hawaii. *J. Volcanol. Geothermal Res.* 207, 16–32. doi: 10.1016/j.jvolgeores.2011.08.001

Sedwick, P. N., McMurtry, G. M., Hilton, D. R., and Goff, F. (1994). Carbon dioxide and helium in hydrothermal fluids from Loihi Seamount, Hawaii, USA: temporal variability and implications for the release of mantle volatiles. *Geochim. Cosmochim. Acta* 58, 1219–1227. doi: 10.1016/0016-7037(94)90587-8

Sedwick, P. N., McMurtry, G. M., and Macdougall, J. D. (1992). Chemistry of hydrothermal solutions from Pele's Vents, Loihi Seamount, Hawaii. *Geochim. Cosmochim. Acta* 56, 3643–3667. doi: 10.1016/0016-7037(92)90159-G

Simkin, T., and Howard, K. A. (1970). Caldera collapse in the Galapagos Islands, 1968. *Science* 169, 429–437. doi: 10.1126/science.169.3944.429

Smith, J. R., Satake, K., and Suyehiro, K. (2002). "Deepwater multibeam sonar surveys along the southeastern Hawaiian Ridge. Guide to the CD-rom," in *Hawaiian Volcanoes: Deep Underwater Perspectives*, Vol. 128, eds E. Takahashi, P. W. Lipman, M. O. Garcia, J. Naka, and S. Aramaki (Washington, DC: American Geophysical Union), 3–9. doi: 10.1029/GM128p0003

Smith, J. R., Shor, A. N., Malahoff, A., and Torresan, M. E. (1994). *Southeast flank of island of Hawaii. Sheet* 4, *Hawaii Seafloor Atlas*. Honolulu: Hawaii Institute of Geophysics and Planetology.

Tibaldi, A., and Vezzoli, L. (1998). The space problem of caldera resurgence: an example from Ischia Island. Italy. *Geologische Rundschau* 87, 53–66. doi: 10.1007/s005310050189

Umino, S., Lipman, P. W., and Obata, S. (2000). Subaqueous lava flow lobes, observed on ROV dives off Hawaii. *Geology* 28, 503–506. doi: 10.1130/0091-7613(2000)28<503:SLFLOO>2.0.CO;2

Umino, S., Obata, S., Lipman, P. W., Smith, J. R., and Shibata, T. (2002). "Emplacement and inflation structures of submarine and subaerial pahoehoe lavas from Hawaii," in *Hawaiian Volcanoes: Deep Underwater Perspectives*, Vol. 128, eds E. Takahashi, P. W. Lipman, M. O. Garcia, J. Naka, and S. Aramakai (Washington, DC: American Geophysical Union), 85–101.

Wanless, V. D., Garcia, M. O., Truesdell, F. A., Rhodes, J. M., Norman, M. D., Weis, D., et al. (2006). Submarine radial vents on Mauna Loa Volcano, Hawaii. *Geochem. Geophys. Geosyst.* 7:Q05001. doi: 10.1029/2005GC001086

Wheat, C. G., Sansone, F. J., McMurtry, G. M., Jannasch, H. W., Plant, J. N., and Moyer, C. L. (2000). Continuous sampling of hydrothermal fluids from Loihi Seamount after the 1996 event. *J. Geophys. Res.* 105, 19353–19367. doi: 10.1029/2000JB900088

Conflict of Interest Statement: The authors declare that the research was conducted in the absence of any commercial or financial relationships that could be construed as a potential conflict of interest.